Tetrahedron 85 (2021) 132065

Contents lists available at ScienceDirect

Tetrahedron

journal homepage: www.elsevier.com/locate/tet

Fusaristatins D–F and (7*S*,8*R*)-(−)-chlamydospordiol from *Fusarium* sp. BZCB-CA, an endophyte of *Bothriospermum chinense*

Ni Putu Ariantari [a, b], Marian Frank [a], Ying Gao [a], Fabian Stuhldreier [c], Anna-Lene Kiffe-Delf [a], Rudolf Hartmann [d], Simon-Patrick Höfert [e], Christoph Janiak [e], Sebastian Wesselborg [c], Werner E.G. Müller [f], Rainer Kalscheuer [a], Zhen Liu [a, g, *], Peter Proksch [a, h, **]

[a] *Institute of Pharmaceutical Biology and Biotechnology, Heinrich Heine University Düsseldorf, Universitätsstrasse 1, 40225, Düsseldorf, Germany*
[b] *Department of Pharmacy, Faculty of Mathematics and Natural Sciences, Udayana University, 80361, Bali, Indonesia*
[c] *Institute of Molecular Medicine I, Medical Faculty and University Hospital Düsseldorf, Heinrich Heine University Düsseldorf, Universitätsstrasse 1, 40225, Düsseldorf, Germany*
[d] *Institute of Biological Information Processing: Structural Biochemistry (IBI-7), Forschungszentrum Jülich GmbH, IBI-7, 52425, Jülich, Germany*
[e] *Institute of Inorganic Chemistry and Structural Chemistry, Heinrich Heine University Düsseldorf, Universitatsstrasse 1, 40225, Düsseldorf, Germany*
[f] *Institute for Physiological Chemistry, University Medical Center of the Johannes Gutenberg University Mainz, Duesbergweg 6, 55128, Mainz, Germany*
[g] *Key Laboratory of Study and Discovery of Small Targeted Molecules of Hunan Province, School of Medicine, Hunan Normal University, Changsha, 410013, PR China*
[h] *Hubei Key Laboratory of Natural Products Research and Development, College of Biological and Pharmaceutical Sciences, China Three Gorges University, Yichang, 443002, PR China*

ARTICLE INFO

Article history:
Received 24 January 2021
Received in revised form
27 February 2021
Accepted 4 March 2021
Available online 8 March 2021

Keywords:
Endophyte
Fusarium sp.
Lipodepsipeptide
Fusaristatin
Cytotoxicity
Antibacterial activity

ABSTRACT

Three new lipodepsipeptides, fusaristatins D–F (**1**–**3**) and a new α-pyrone derivative, (7*S*,8*R*)-(−)-chlamydospordiol (**5**), together with eight known compounds (**4**, **6**–**12**) were obtained from solid rice cultures of *Fusarium* sp. BZCB-CA, an endophyte of the Chinese medicinal plant, *Bothriospermum chinense*. The planar structures of the new metabolites (**1**–**3**, **5**) were established by spectroscopic techniques (1D/2D NMR and HRESIMS). Marfey's method was applied to determine the absolute configuration of **1**, while the absolute configuration of **5** was determined by single-crystal X-ray crystallography analysis in addition to Mosher's method. Crystallographic data of inflatin C (**7**) are also supplied here for the first time. In cytotoxicity assays, rubrofusarin (**8**) showed a moderate effect on the lymphoma cell lines L5178Y, Ramos and Jurkat, with IC_{50} values of 7.7, 6.2 and 6.3 μM, respectively, while the remaining compounds were inactive. When subjected to antibacterial assay, only lateropyrone (**9**) exhibited good to weak activity against a panel of Gram-positive bacteria including drug-resistant strains with MICs ranging from 3.1 to 25 μM.

1. Introduction

Members of the genus *Fusarium* are widely distributed in nature as soil inhabitants and plant-associated microorganisms [1]. Among filamentous fungi, *Fusarium* spp. are recognized as excellent producers of numerous chemically interesting secondary metabolites with promising bioactivities [2]. For example, enniatins, cyclohexadepsipeptides produced by some species of *Fusarium*, displayed a wide range of bioactivities as antimicrobial, antifungal and anticancer activities, which are related to their ionophoric properties [3,4]. Notably, a pharmaceutical product containing a mixture of enniatins A–C, fusafungine, once has been marketed for the treatment of upper respiratory tract infections, before it was withdrawn in 2016 due to serious allergic reactions [5]. Although several *Fusarium* species were frequently identified as plant

* Corresponding author. Institute of Pharmaceutical Biology and Biotechnology, Heinrich Heine University Düsseldorf, Universitätsstrasse 1, 40225, Düsseldorf, Germany.
** Corresponding author. Institute of Pharmaceutical Biology and Biotechnology, Heinrich Heine University Düsseldorf, Universitätsstrasse 1, 40225, Düsseldorf, Germany.
E-mail addresses: zhenfeizi0@sina.com (Z. Liu), proksch@uni-duesseldorf.de (P. Proksch).

https://doi.org/10.1016/j.tet.2021.132065
0040-4020/

pathogens contributing to destructive plant diseases such as banana wilt [6,7], and head blight of wheat [8,9], many others were reported to demonstrate an endophytic lifestyle pertaining to their mutualistic relationship with the host plants [10–12].

During the course of our continuous search for bioactive natural products from fungal endophytes, *Fusarium* sp. BZCB-CA was obtained from healthy stem tissue of *Bothriospermum chinense* (Boraginaceae). Diverse biologically active natural products have been isolated from *Fusarium* endophytes, including the immunosuppressive subglutinols A and B [13], antimycobacterial and cytotoxic dihydronaphtalenone [14], and antimicrobial fusariumins B–D [15–17]. In the present study, subsequent chromatographic separation of the crude EtOAc extract of the strain cultivated on solid rice medium, resulted in 12 natural products (**1**–**9**, Fig. 1), of which four are new metabolites (**1**–**3**, **5**). Herein, we describe the isolation and structure elucidation of three new lipodepsipeptides, fusaristatins D–F (**1**–**3**) and (7*S*,8*R*)-(−)-chlamydospordiol (**5**), as well as the result of cytotoxic and antibacterial assays.

2. Result and discussions

Fusaristatin D (**1**) was obtained as a white, amorphous solid. The molecular formula, $C_{36}H_{58}N_4O_8$, was determined by HRESIMS, corresponding to ten degrees of unsaturation. Comparison of ^{1}H and ^{13}C NMR data of **1** (Table 1) to those of fusaristatin A (**4**) [18], co-isolated in this study, revealed close similarity of both compounds except for the presence of signals attributed to an oxygenated methine at δ_H 2.91/δ_C 65.2 (C-10) and an oxygenated quaternary carbon at δ_C 58.1 (C-11) in **1**. A continuous spin system observed in the COSY spectrum from H_3-1 until H-10, along with detected HMBC correlations from H-10 to C-11 and C-12, as well as from H_3-11′ to C-10, C-11, and C-12 (Fig. 2), indicated the presence of an epoxy group between C-10 and C-11, instead of a double bond at the same position in fusaristatin A, which was further supported by its molecular formula, bearing one more oxygen compared to fusaristatin A. The remaining partial structure of **1** was concluded to be the same as that of fusaristatin A (**4**), based on detailed analysis of its 2D NMR data (Fig. 2). The large coupling constant (15.9 Hz) suggested *E* configuration for the double bond at C-12/C-13. The absolute configuration of the epoxide in **1** could not be unambiguously assigned, however, *trans* configuration between H-

Table 1
^{1}H and ^{13}C NMR data (DMSO-d_6) of compounds **1** and **2**.

NO.	1[a]			2[a]		
	δ_C, type		δ_H (*J* in Hz)	δ_C, type[b]		δ_H (*J* in Hz)
1	13.7	CH_3	0.85, t (7.1)	13.8	CH_3	0.85, t (7.0)
2	21.9	CH_2	1.26, m	21.9	CH_2	1.26, m
3	31.2	CH_2	1.23, m	31.1	CH_2	1.22, m
4	28.8	CH_2	1.23, m	28.7	CH_2	1.23, m
5	26.2	CH_2	1.27, m	26.1	CH_2	1.23, m
6	36.2	CH_2	1.26, m; 1.09, m	36.0	CH_2	1.23, m; 1.06, m
7	31.8	CH	1.42, m	31.6	CH	1.36, m
7′	19.2	CH_3	0.84, d (6.5)	19.2	CH_3	0.79, d (6.6)
8	32.7	CH_2	1.44, m; 1.17, m	32.5	CH_2	1.40, m; 1.28, m
9	25.5	CH_2	1.58, m; 1.52, m	25.0	CH_2	1.48, m; 1.41, m
10	65.2	CH	2.91, t (6.2)	65.9	CH	3.04, t (6.3)
11	58.1	C		59.4	C	
11′	14.6	CH_3	1.40, s	20.7	CH_3	1.42, s
12	148.1	CH	6.58, d (15.9)	143.6	CH	6.76, d (15.9)
13	127.7	CH	6.37, d (15.9)	129.4	CH	6.33, d (15.9)
14	202.1	C		202.0	C	
15	42.7	CH	2.79, m	42.6	CH	2.81, m
15′	15.9	CH_3	0.97, d (6.8)	16.0	CH_3	0.98, d (6.9)
16	26.7	CH_2	1.55, m; 1.24, m	26.5	CH_2	1.56, m; 1.26, m
17	28.2	CH_2	1.60, m; 1.45, m	28.1	CH_2	1.62, m; 1.46, m
18	75.4	CH	4.88, m	75.2	CH	4.88, m
19	42.6	CH	2.67, m	42.5	CH	2.67, m
19′	14.3	CH_3	1.06, d (7.3)	14.3	CH_3	1.07, d (7.2)
20	172.2	C		172.4	C	
21		NH	9.29, s		NH	9.30, s
22	137.1	C		137.2	C	
22′	115.3	CH_2	5.79, s; 5.29, s	115.4	CH_2	5.79, s; 5.28, s
23	163.1	C		163.3	C	
24		NH	6.65, t (6.0)		NH	6.67, t (5.8)
25	41.3	CH_2	3.31, m	41.2	CH_2	3.31, m
26	40.8	CH	2.46, m	40.7	CH	2.46, m
26′	14.5	CH_3	1.05, d (7.2)	14.4	CH_3	1.06, d (7.3)
27	173.1	C		173.2	C	
28		NH	8.04, d (8.0)		NH	8.03, d (7.9)
29	51.4	CH	4.23, m	51.3	CH	4.24, m
30	170.6	C		170.7	C	
31	25.8	CH_2	2.00, m; 1.90, m	25.6	CH_2	1.99, m; 1.91, m
32	31.1	CH_2	2.07, t (7.9)	31.0	CH_2	2.06, t (8.0)
33	173.4	C		173.5	C	
34		NH_2	7.27, s; 6.76, s		NH_2	7.25, s; 6.73, s

[a] Measured at 700 MHz (^{1}H) and 175 MHz (^{13}C).
[b] Chemical shifts were extracted from HSQC and HMBC.

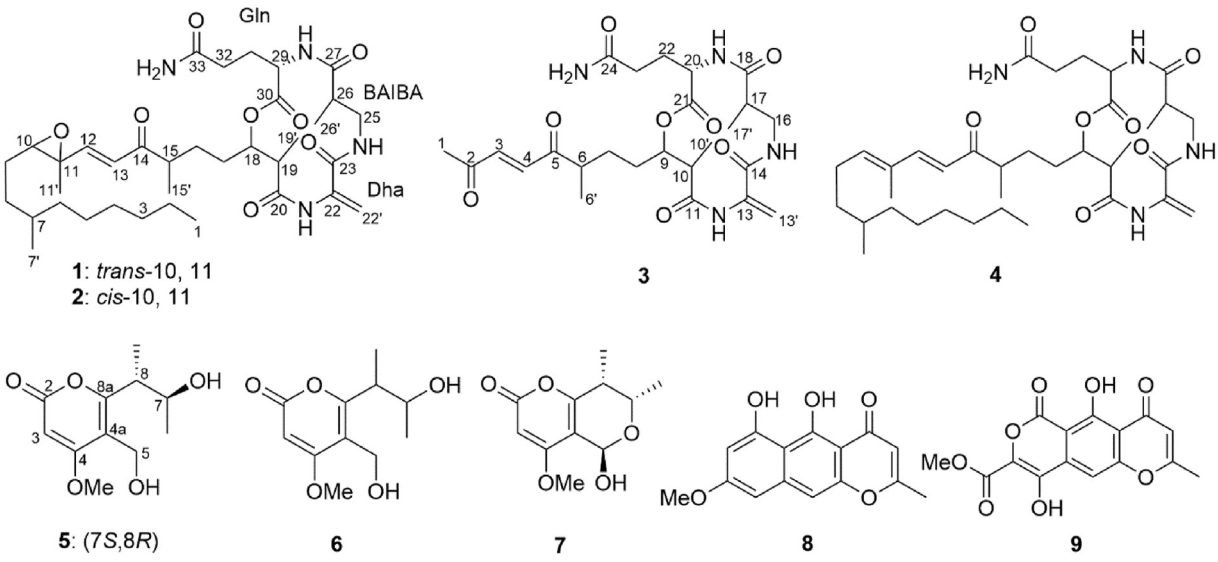

Fig. 1. Structures of compounds **1**–**9** isolated from *Fusarium* sp. BZCB-CA.

10 and H_3-11′, was proposed based on strong NOE correlations between H-10/H-12 and between H_3-11/H-13 in addition to lack of NOE correlation between H-10/H_3-11'. The peptide backbone of **1** was constructed of dehydroalanine (Dha), β-amino isobutyric acid (BAIBA) and glutamine (Gln), identical to that of fusaristatin A. The configuration of Gln residue, however, had never been reported before [18]. To determine the absolute configuration of Gln, the acid hydrolysate of **1** was derivatized with Marfey's reagent. As a result, L-FDAA amino acid derivative of **1** eluted earlier than its D-FDAA derivative, in accordance with the elution order of FDAA derivatives of amino acid standards L-Glu eluted prior to D-Glu, allowing the assignment of L-Gln residue in **1**. Thus, compound **1** was established as an epoxide analogue of fusaristatin A.

Fusaristatin E (**2**) displayed the same molecular formula as that of **1**. The ^{1}H and ^{13}C NMR data of **2** (Table 1) resembled those of **1**. Detailed analysis of the 2D NMR spectra of **2** indicated that both compounds share the same planar structure. *E* configuration was assigned for the double bond at C-12/C-13 on the basis of the large value of $J_{H\text{-}12/H13}$ (15.9 Hz). However, H-10 (+0.13 ppm), C-11 (1.3 ppm), C-11' (6.1 ppm) and H-12 (+0.18 ppm) were shifted downfield whereas C-12 (−4.5 ppm) was shifted upfield in **2** when compared to **1**, suggesting configurational change in the epoxy moiety. The ROESY spectrum of **2** showed the presence of a cross peak correlation between H-10/H_3-11′, which was absent in **1**, suggesting *cis* relationship between C10 and C-11' in compound **2**. Thus, the relative stereochemistry of the epoxide in the unsaturated side chain distinguished the structure of **2** from that of **1**.

The molecular formula of fusaristatin F (**3**) was deduced as $C_{25}H_{36}N_4O_8$ from HRESIMS data, indicating ten degrees of unsaturation. Detailed analysis of its 1D/2D NMR data revealed that **3** bears the same partial structure with regard to the cyclic part of the molecule including the peptide backbone as those of compounds **1** and **2**. However, differences of signals in the ^{1}H NMR data of **3** (Table 2) attributed to the unsaturated aliphatic side chain were observed. Signals corresponding to two methyl groups, seven sets of methylene and two methine protons in the side chain detected in the ^{1}H NMR data of **1** and **2** disappeared in **3**. Instead, a downfield shifted methyl singlet resonating at δ_H 2.36 (H_3-1) was observed in the latter compound. This evidence suggested that **3** bears a shorter side chain than that of the aforementioned analogues, as supported by its molecular formula. The HMBC correlations from H_3-1 to C-3 and the keto function at C-2, and from H_3-6′, H-3 and H-4 to the carbonyl C-5, together with consecutive COSY correlations from H_3-6′ through to H_3-10', indicated the presence of a 3-octene-2,5-dione-6-methyl moiety as side chain of **3**. Hence, the planar structure of **3** was elucidated as shown (Fig. 1). According to recent biosynthetic studies on fusaristatin A, a polyketide synthase *PKS6* starts the production of the lipid portion of the molecule, which is then assembled to the sequence of three amino acid residues (Dha, BAIBA and L-Gln) by a nonribosomal peptide synthetase *NRPS7* [19,20]. The known fusaristatins A and B bear side chain characterized by the presence of arachidic acid structure, which is epoxidized at $\Delta^{10(11)}$ in the case of **1** and **2**. The biosynthesis pathway of epoxide-containing natural products are well described in the literature [21]. In general, the formation of epoxide would require O_2 to supply oxygen atom or act as an oxidizing agent. Molecular oxygen (O_2) would be converted to form reactive oxygen species which could react with many biomolecules. This process may involve some biosynthetic enzymes, such as P450-dependent epoxidases or flavin-dependent epoxidases, which could facilitate the insertion of oxygen atom into the double bond, forming an epoxide.

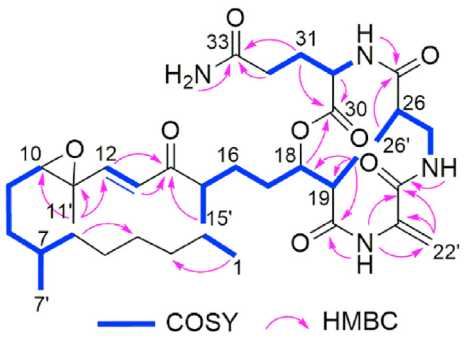

Fig. 2. Key COSY and HMBC correlations of **1**.

Table 2
^{1}H and ^{13}C NMR data (DMSO-d_6) of compound **3**.

position	3[a]		
	δ_C, type[b]		δ_H (J in Hz)
1	27.8	CH_3	2.36, s
2	198.8	C	
3	136.9	CH	6.77, d (16.2)
4	136.0	CH	7.05, d (16.2)
5	203.5	C	
6	43.3	CH	2.94, m
6′	15.4	CH_3	1.03, d (7.0)
7	26.2	CH_2	1.61, m; 1.28, m
8	27.9	CH_2	1.65, m; 1.46, m
9	75.1	CH	4.90, m
10	42.5	CH	2.69, m
10′	14.2	CH_3	1.08, d (7.2)
11	172.1	C	
12		NH	9.28, s
13	137.0	C	
13′	115.3	CH_2	5.79, s; 5.29, s
14	163.0	C	
15		NH	6.65, t (5.8)
16	41.1	CH_2	3.31, m
17	40.6	CH	2.46, m
17′	14.4	CH_3	1.06, d (7.3)
18	173.0	C	
19		NH	8.02, d (7.8)
20	51.2	CH	4.24, m
21	170.5	C	
22	25.5	CH_2	2.00, m; 1.91, m
23	30.9	CH_2	2.07, t (8.0)
24	173.3	C	
25		NH_2	7.26, s; 6.74, s

[a] Measured at 700 MHz (^{1}H) and 175 MHz (^{13}C).
[b] Chemical shifts were extracted from HSQC and HMBC.

Compound **5** was obtained as colorless crystals. The molecular formula of **5** was determined as $C_{11}H_{16}O_5$ by analysis of its HRESIMS data, requiring four degrees of unsaturation. Its UV spectrum showed a characteristic UV pattern with maximum absorption around 282 nm, indicative for the presence of a conjugated α-pyrone nucleus [22,23]. Five sp [2] hybridized carbons resonating at δ_C 170.0, 164.3, 163.8, 112.8 and 88.3, observed in the ^{13}C NMR spectrum were assigned to the α-pyrone core in the structure of **5**. Furthermore, the ^{1}H NMR and ^{13}C NMR data of **5** (Table 3) displayed signals of an olefinic singlet, two doublet methyl groups, two methines, one methoxy and an isolated oxygenated methylene. The latter two signals were attached to C-4 and C-4a in the α-pyrone through their respective HMBC correlations. The presence of a 2-butanol side chain at C-8a was evident from COSY correlations between 8-Me/H-8/H-7/7-Me and HMBC correlations 8-Me to C-8a and from H-8 to C-4a. Thus, compound **5** was elucidated to share the same planar structure as that of chlamydospordiol (**6**) [24], co-isolated in this study. However, the chemical shifts in the 2-butanol side chain in **5** obviously differed from those in **6**. Moreover, J value

Table 3
^{1}H and ^{13}C NMR data ($CDCl_3$) of compound **5**.[a]

position	5		
	δ_C, type		δ_H (*J* in Hz)
2	163.8	C	
3	88.3	CH	5.49, s
4	170.0	C	
4a	112.8	C	
5	54.0	CH_2	4.55, d (12.5); 4.36, d (12.5)
7	70.2	CH	4.02, qd (6.4, 5.2)
8	41.0	CH	3.23, qd (7.1, 5.2)
4-OMe	56.4	CH_3	3.87, s
7-Me	19.7	CH_3	1.21, d (6.4)
8-Me	14.4	CH_3	1.30, d (7.1)

[a] Measured at 600 MHz (^{1}H) and 150 MHz (^{13}C).

between these two vicinal protons of 5.2 Hz was found for **5**, in comparison to 9.0 Hz obtained for **6**, suggesting the relative configuration at C-7 and C-8 to be different in both compounds. Even though chlamydospordiol (**6**) was isolated more than twenty years ago from *Fusarium chlamydosporum* and *Fusarium tricinctum* [24], no report addressing its absolute configuration had been published before.

In an attempt to resolve the stereochemistry of compound **5**, Mosher's method employing (*R*) and (*S*)-MTPA-Cl was carried out to determine the absolute configuration of C-7, yielding either (*S*) and (*R*)-MTPA ester products of **5**. The proposed Mosher's model [25] was applied following the calculation of $\Delta\delta^{SR}$ of MTPA esters of **5**, allowing the assignment of C-7 stereocenter as (*S*) configuration (Fig. 3). Moreover, the absolute structure of compound **5** was determined by anomalous dispersion from Cu-K_α radiation to (7*S*,8*R*) as depicted in Fig. 4. In contrast to **5**, Mosher's reaction on chlamydospordiol (**6**) failed. As a sufficient quality of crystal for **6** could not be achieved, the absolute configuration of chlamydospordiol (**6**) remains unassigned.

Single-crystal X-ray crystallography was also able to provide the crystal structure of inflatin C (**7**) (Fig. S38 in Supporting Information), supporting the structure reported earlier for this compound obtained from the soil-derived fungus, *Tolypocladium inflatum* [26]. The remaining known compounds were identified as rubrofusarin (**8**) [27,28], lateropyrone (**9**) [10], enniatins A (**10**), A1 (**11**), and B1 (**12**) [29–31], based on comparison of their spectroscopic data (NMR and ESIMS) and specific optical rotation to those in the literature, as well as by co-chromatography with reference compounds for lateropyrone and enniatins.

Compounds **1**–**9** were subjected to cytotoxicity assays against

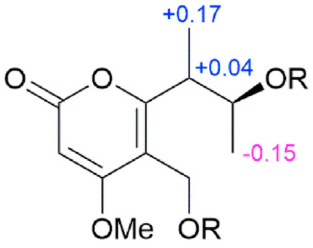

5a : R = (*S*)-MTPA
5b : R = (*R*)-MTPA

Fig. 3. $\Delta\delta^{SR}$ values in ppm for the MTPA esters of **5**.

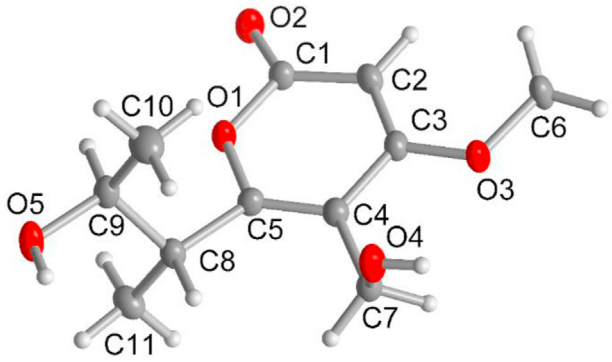

Fig. 4. Molecular structure of compound **5** from single-crystal X-ray analysis.

the murine lymphoma cell line L5178Y. In this assay, rubrofusarin (**8**) was moderately cytotoxic with an IC_{50} value of 7.7 μM, while the remaining compounds were inactive. When tested further for cytotoxicity against two human lymphoma cell lines, Ramos and Jurkat J16, rubrofusarin (**8**) exhibited moderate cell growth inhibition after 72 h of action time with IC_{50} values of 6.2 and 6.3 μM, respectively.

Moreover, compounds **1**–**9** were evaluated for antibacterial activity against a panel of Gram-positive and Gram-negative strains. Among them, only lateropyrone (**9**) showed growth inhibition against *Staphylococcus aureus*, *Enterococcus faecalis*, and *Enterococcus faecium*, including methicillin-resistant of *S. aureus* (MRSA) and vancomycin-resistant of *E. faecalis* and *E. faecium*, with MIC values of 3.1, 12.5 and 25 μM, respectively. This result is consistent with previous reports [10]. None of the tested compounds showed activity against *Mycobacterium tuberculosis* H37Rv up to a concentration of 100 μM. Albeit found inactive in our assay, rubrofusarin (**8**) has been reported previously to possess antimycobacterial activity against *M. tuberculosis* (ATCC 27294) with MIC value of 12 μg/mL [27]. Rubrofusarin (**8**) has also been reported for its inhibitory effect against human DNA topoisomerase II-α, with the activity comparable to that of the reference drug, etoposide [28]. This report is in line with our finding on cytotoxic activity of rubrofusarin (**8**) against the tested cell lines in the present study, suggesting inhibition of DNA topoisomerase as one possible mode of action of its cytotoxicity. More recently, rubrofusarin (**8**) was investigated as an inhibitor of amyloid β (Aβ) aggregation in an Alzheimer's disease mouse model [32], as well as for its dual inhibitory activities against protein tyrosine phosphate 1 B (PTP1B) and human monoamine oxidase A (hMAO-A) [33].

The new cyclic lipodepsipeptides **1**–**3**, display similar structural features as those of reported for topostatin isolated from thermophilic actinomycete strain *Thermomonospora alba* [34–36], YM-170320, an acyclic analogue derived from an unidentified fungus [37], and fusaristatins A–C produced by *Fusarium* sp. YG-45,[18] and *Pithomyces* sp. RKDO 1698 [38]. Topostatin [36] and fusaristatin B [18] were found previously to inhibit topoisomerase I and II, while YM-170320 moderately induced the morphological changes of a mutant strain of *Candida tropicalis* [37]. Fusaristatin A was investigated before for its antifungal properties against *Fusarium solani*, *Saccharomyces cerevisiae*, *Penicillium chrysogenum* and *Scopulariopsis brevicaulis*, however it was inactive up to a concentration of 100 μM [19]. Additionally, fusaristatins A and B showed cytotoxic activity against lung cancer cells (LU 65) with IC_{50} values of 23 and 7 μM, respectively [18], although none of the new analogues (**1**–**3**) encountered in this study exhibited cytotoxicity or antimicrobial

activities.

3. Experimental section

3.1. General procedures

HPLC analysis was conducted using a Dionex UltiMate 3000 system with an UltiMate 3000 pump connected to a photodiode array detector (DAD 3000 RS, UV detection at 235, 254, 280 and 340 nm) on a Eurospher 100-10C_{18} column (125 × 4 mm, Knauer, Germany). Semipreparative HPLC was carried out with a Merck Hitachi Chromaster HPLC system (UV detector 5410; pump 5110; column Eurospher 100-10C_{18}, 300 × 8 mm, Knauer, Germany; flow rate at 5 mL/min). Silica 60 M (0.040–0.063 mm; Macherey-Nagel, Germany) and Sephadex LH-20 were used for column chromatography. TLC analysis was performed on silica gel 60 F_{254} TLC plates (Macherey-Nagel, Germany), and visualized under UV detection at 254 and 366 nm. 1D and 2D NMR spectra were recorded on Bruker AVANCE III HD 700, 600, and DMX 300 NMR spectrometers. The chemical shifts (δ) were referenced to residual solvent signals at δ_H 3.31 (MeOH-d_4), 2.50 (DMSO-d_6) and 7.26 ($CDCl_3$) ppm for ^{1}H, δ_C 49.0 (MeOH-d_4), 39.5 (DMSO-d_6) and 77.0 ($CDCl_3$) ppm for ^{13}C. ESI and HRESIMS spectra were measured with a Finnigan LCQ Deca and a UHR-QTOF maXis 4G (Bruker Daltonics) mass spectrometers. Optical rotations were obtained on a Jasco P-2000 polarimeter.

3.2. Fungal material and cultivation

The fungus *Fusarium* sp. BZCB-CA, was isolated from healthy stem tissue of *Bothriospermum chinense* (Boraginaceae) [39], collected in Beijing, People's Republic of China, in April 2018. The standard molecular biology procedure and sequencing on ITS region (ITS 1 and 4), followed by nucleotide BLAST search in the NCBI database, was adopted for the fungal identification [39]. The sequence was submitted to the GenBank (accession no. MN493761). The culture strain is kept in the Institute of Pharmaceutical Biology and Biotechnology, Heinrich Heine University, Düsseldorf, Germany. The fungus was then cultivated on sterile rice medium in ten 1 L flasks, prepared by autoclaving 100 g of rice in 100 mL distilled water at 121 °C for 20 min. The fungal culture was allowed to grow under the static condition at 20 °C, until the fungus thoroughly covered the rice medium.

3.3. Extraction and isolation

At the end of the fermentation, each culture flask was soaked with 500 mL EtOAc and shaken continuously at 150 rpm for 10 h. After filtration through filter paper, the resulting extract was concentrated under vacuum to dryness. The obtained crude extract (7.5 g) was subjected to vacuum liquid chromatography (VLC) on Silica 60 M material, employing *n*-hexane-EtOAc and CH_2Cl_2–MeOH as solvent system through a step gradient elution, to afford 14 fractions (V1–V14). Based on HPLC analysis, further separation was performed on fractions V3, V4, V9, and V10, eluted with *n*-hexane-EtOAc (4:6, 6:4), CH_2Cl_2–MeOH (9:1, 7:3), respectively. Fraction V3 (696 mg) was subjected to a Sephadex LH-20 column and eluted with CH_2Cl_2–MeOH (1:1), followed by purification with semipreparative HPLC using MeOH–H_2O (from 30% to 70% MeOH, 14 min), resulted in **7** (4.6 mg). Meanwhile, fraction V4 (945 mg), was gently rinsed with MeOH to give red-brownish crystals **8** (65.0 mg) and MeOH soluble portion. The latter was chromatographed further over a Sephadex LH-20 column using CH_2Cl_2–MeOH (1:1) as mobile phase to give 7 subfractions (V4.1–V4.7). Purification on subfraction V4.2 (77 mg) was done by semipreparative HPLC through gradient elution of MeOH–H_2O (from 80% to 100% MeOH, 16 min) to afford **10** (28.9 mg), **11** (14.4 mg) and **12** (2.7 mg). In a similar way, compounds **5** (30.5 mg), **6** (27.2 mg) and **9** (3.1 mg) were obtained by separation of fraction V9 (635 mg) on a Sephadex LH-20 column and followed by purification using semipreparative HPLC eluted with MeOH-0.1% HCOOH in H_2O (from 15% to 45% MeOH for 14 min, and from 50% to 100% MeOH for 14 min). Following a similar procedure, compounds **1** (3.5 mg), **2** (1.5 mg), **3** (2.0 mg) and **4** (15.0 mg) were obtained after chromatographic workup on fraction V10 (489 mg) over a Sephadex LH-20 column with CH_2Cl_2–MeOH (1:1) as eluent and semipreparative HPLC using MeOH–H_2O (from 30% to 100% MeOH, 25 min) as a mobile phase.

Fusaristatin D (**1**): a white, amorphous solid; [α]20 D −32 (*c* 0.10, MeOH); UV (MeOH): λ_{max} 230 nm; ^{1}H and ^{13}C NMR data, see Table 1; HRESIMS *m/z* 675.4317 $[M + H]^+$ (calcd for $C_{36}H_{59}N_4O_8$, 675.4327).

Fusaristatin E (**2**): a white, amorphous solid; [α]20 D −30 (*c* 0.10, MeOH); UV (MeOH): λ_{max} 227 nm; ^{1}H and ^{13}C NMR data, see Table 1; HRESIMS *m/z* 675.4331 $[M + H]^+$ (calcd for $C_{36}H_{59}N_4O_8$, 675.4327).

Fusaristatin F (**3**): a white, amorphous solid; [α]20 D −36 (*c* 0.10, MeOH); UV (MeOH): λ_{max} 229 nm; ^{1}H and ^{13}C NMR data, see Table 2; HRESIMS *m/z* 521.2605 $[M + H]^+$ (calcd for $C_{25}H_{37}N_4O_8$, 521.2606).

(7*S*,8*R*)-(−)-Chlamydospordiol (**5**): colorless, crystals; [α]20 D−104 (*c* 0.20, MeOH); UV (MeOH): λ_{max} 282 and 206 nm; ^{1}H and ^{13}C NMR data, see Table 3; HRESIMS *m/z* 229.1072 $[M + H]^+$ (calcd for $C_{11}H_{17}O_5$, 229.1071).

3.4. Mosher ester analysis of **5**

Mosher's reaction for compound **5** was performed as described before [23,40]. Two solutions, each containing 1.0 mg (4.4 μmol) of **5** in 100 μL $CDCl_3$, were transferred into two NMR tubes. Accordingly, 10 μL (*R*)-MTPA-Cl (53.4 μmol) was added to the first solution and 10 μL (*S*)-MTPA-Cl (53.4 μmol) was included to the second solution. Both reaction mixtures were allowed to stand at room temperature for 3 h, followed by addition of 500 μL $CDCl_3$ to each solution. ^{1}H NMR and COSY spectra of (*S*)- and (*R*)-MTPA esters were recorded. Both ester products were evaporated *in vacuo* and purified by semipreparative HPLC using MeOH-0.1% HCOOH in H_2O as a mobile phase by gradient elution from 70% to 100% MeOH over 14 min. The resulting (*S*)- and (*R*)-MTPA esters were then subjected to ESIMS analysis, both showed the prominent peaks at *m/z* 683 $[M + Na]^+$, indicating either primary or secondary OH groups in **5** were reacted with Mosher's reagents.

(*S*)-MTPA ester of 5 (5a): ^{1}H NMR ($CDCl_3$, 600 MHz) δ_H 5.44 (1H, s, H-3), 5.23 (1H, dq, J = 8.1, 6.2 Hz, H-7), 5.09 (1H, d, J = 12.4 Hz, Ha-5), 4.95 (1H, d, J = 12.4 Hz, Hb-5), 3.15 (1H, dq, J = 8.1, 6.8 Hz, H-8), 1.18 (3H, d, J = 6.8 Hz, H_3-8), 1.05 (3H, d, J = 6.2 Hz, H_3-7).

(*R*)-MTPA ester of 5 (5b): ^{1}H NMR ($CDCl_3$, 600 MHz) δ_H 5.42 (1H, s, H-3), 5.25 (1H, dq, J = 8.4, 6.2 Hz, H-7), 4.98 (1H, d, J = 12.4 Hz, Ha-5), 4.94 (1H, d, J = 12.4 Hz, Hb-5), 3.11 (1H, dq, J = 8.4, 6.8 Hz, H-8), 1.20 (3H, d, J = 6.2 Hz, H_3-7), 1.01 (3H, d, J = 6.8 Hz, H_3-8).

3.5. Marfey's reaction of **1**

The previously described procedure for C_3 Marfey's method was adopted [41,42]. Two samples, each containing 0.2 mg (0.3 μmol) of **1**, were hydrolyzed with 100 μL 6 M HCl in two sealed glass vials and incubated at 110 °C for 8 h. Afterwards, hydrolysates were concentrated *in vacuo*. To each hydrolysate, 20 μL 1 M $NaHCO_3$ was included, followed by addition of each 40 μL (1.5 μmol) of 1% solution of D- or L-FDAA in acetone and both solutions were maintained at 40 °C for 1 h. The same procedure was done for the amino

acid standards L-glutamic acid (L-Glu) and DL-glutamic acid (DL-Glu). The reaction was stopped by adding 20 μL 1 M HCl to each reaction mixtures and 10 μL of each analyte was injected for HPLC analysis. For the analysis, MeOH-0.1% HCOOH in H_2O was used as a mobile phase, by gradient elution from 20% to 60% MeOH over 55 min, at flow rate of 1 mL/min, on a Knauer Eurospher 100-10C_{18} column, 125 × 4 mm, and detection at 340 nm. LC-MS analysis was further performed to confirm D- and L-FDAA products of **1**.

3.6. X-ray crystallographic analysis

Crystals were obtained from methanol solution by slow evaporation method. Under a polarizing microscope, suitable crystals were carefully selected and placed in protective oil. A crystal of sufficient quality was measured with a Bruker Kappa APEX2 CCD diffractometer with microfocus tube using Cu-K_α radiation ($\lambda = 0.71073$ Å). For data collection APEX2 [43], for cell refinement SAINT [43], and for experimental absorption correction SADABS was used [44]. The structure was solved with SHELXT by intrinsic phasing and refined with SHELXL-2017 by full-matrix least-squares on *F* [*2*]. [45,46] All hydrogen atoms were positioned geometrically (with C—H = 0.95 Å for aromatic CH, 1.00 Å for tertiary CH, 0.99 Å for CH_2 and 0.98 Å for CH_3) and refined using riding models (AFIX 43, 13, 23 and 137) with U_{iso} (H) = 1.2U_{eq} (CH, CH_2) and 1.5U_{eq} (CH_3). The hydrogen atoms for OH were found and refined free with U_{iso}(H) = 1.5U_{eq}.

The absolute structure of **5** and **7** were determined by anomalous dispersion from Cu-K_α radiation. In both cases, low Friedel Pair coverage made a Bayesian statistics analysis of Bijvoet pair differences necessary [47—49]. The drawing of all graphics was done in DIAMOND [50]. The analyses of hydrogen bonds and Bijvoet pairs was done in PLATON for Windows [51—53]. The structures have been deposited in the Cambridge Crystallographic Data Center (CCDC No. 1968536 (**5**) and 1968535 (**7**)).

Crystal Data of **5**: $C_{10}H_{14}O_3$, M = 182.21, monoclinic system, space group $P2_1$, $a = 6.0350(4)$ Å, $b = 8.0068(6)$ Å, $c = 12.2590(8)$ Å, $V = 574.35(7)$ Å^3, $Z = 2$, $D_{calc} = 1.320$ g/cm^3, crystal size 0.30 × 0.10 × 0.075 mm, μ(Cu Ka) = 0.88 mm^{-1}, 3.7° < θ < 66.6°, $N_t = 6435$, $N = 1758$ ($R_{int} = 0.018$), $R_1 = 0.021$, w$R_2 = 0.058$, $S = 1.06$, Flack parameter x = 0.22(16), Hooft parameter = 0.18(4), probability for correct absolute structure *P*2(true) = 1.000, probability for wrong absolute structure *P*3(false) = $0.3 \cdot 10^{-101}$.

Crystal Data of **7**: $C_{11}H_{14}O_5 \cdot H_2O$, M = 244.24, monoclinic system, space group $P2_1$, $a = 4.7917(3)$ Å, $b = 11.4801(8)$ Å, $c = 10.8081(7)$ Å, $V = 584.61(7)$ Å^3, $Z = 2$, $D_{calc} = 1.387$ g/cm^3, crystal size 0.15 × 0.10 × 0.10 mm, μ(Cu Ka) = 0.97 mm^{-1}, 4.2° < θ < 66.6°, $N_t = 5755$, $N = 1881$ ($R_{int} = 0.027$), $R_1 = 0.027$, w$R_2 = 0.077$, $S = 1.10$, Flack parameter x = 0.10(6), Hooft parameter = 0.11(5), probability for correct absolute structure *P*2(true) = 1.000, probability for wrong absolute structure *P*3(false) = $0.1 \cdot 10^{-62}$.

3.7. Cytotoxicity assay

Cytotoxicity was evaluated against the murine lymphoma cell line L5178Y using the MTT method [54], whereas the activity against the human cell lines Ramos (Burkitt's lymphoma B cells) and Jurkat J16 (adult lymphoblastic leukemia T cells) was carried out by resazurin reduction assay (Alamar blue assay) as previously described [54]. As a negative control, culture medium containing 0.1% DMSO was used. Kahalalide F (IC_{50} = 4.3 μM) was used as a positive control for the cytotoxicity assay against L5178Y cells, while staurosporine (2.5 μM) was included as positive control in the assay towards Ramos and Jurkat J16 cells.

3.8. Antibacterial screening

A panel of the following bacterial strains was employed for antibacterial assay, such as *Mycobacterium tuberculosis* H37Rv, *Staphylococcus aureus* (ATCC 29213 and ATCC 700699), *Enterococcus faecalis* (ATCC 29212 and ATCC 51299), *Enterococcus faecium* (ATCC 35667 and ATCC 700221), *Acinetobacter baumannii* (ATCC BAA1605) and *Pseudomonas aeruginosa* (ATCC 27853). Antibacterial screening of compounds **1**–**9** was carried out by the broth microdilution method under the CLSI guidelines [55], while the activity against *M. tuberculosis* H37Rv was evaluated by the resazurin dye reduction method [56]. Moxifloxacin was included as positive control for all tested Gram-positive and Gram-negative bacteria, except for the assay involving *M. tuberculosis*, which used rifampicin as a positive control. The tested natural products were pre-dissolved in DMSO and medium containing 1% DMSO was used as a negative control.

Declaration of competing interest

The authors declare that they have no known competing financial interests or personal relationships that could have appeared to influence the work reported in this paper.

Acknowledgements

Financial support by the German Academic Exchange Service (DAAD) to N.P.A. is gratefully acknowledged. This work was supported by the Deutsche Forschungsgemeinschaft (DFG, German Research Foundation) — project number 270650915/GRK 2158 (to P.P., S.W. and R.K.) and RTG 2578 (to S.W.) and the Duesseldorf School of Oncology (funded by the Comprehensive Cancer Center Duesseldorf/ Deutsche Krebshilfe and the Medical Faculty of the Heinrich Heine University Duesseldorf; to S.W.). The authors acknowledge access to the Juelich-Duesseldorf Biomolecular NMR Center that is jointly run by Forschungszentrum Juelich and Heinrich-Heine-Universitaet Duesseldorf

Appendix A. Supplementary data

Supplementary data to this article can be found online at https://doi.org/10.1016/j.tet.2021.132065.

References

[1] B.A. Summerell, J.F. Leslie, Fungal Divers. 50 (2011) 135—144.
[2] R.M.K. Toghueo, Mycology 1—21 (2019).
[3] A.A. Sy-Cordero, C.J. Pearce, N.H. Oberlies, J. Antibiot. 65 (2012) 541—549.
[4] G. Meca, J. Soriano, A. Gaspari, A. Ritieni, A. Moretti, J. Mañes, Toxicon 56 (2010) 480—485.
[5] K. Hedenmalm, X. Kurz, D. Morales, Eur. J. Clin. Pharmacol. 75 (2019) 979—984.
[6] C.Y. Li, G. Mostert, C.W. Zuo, I. Beukes, Q.S. Yang, O. Sheng, R.B. Kuang, Y.R. Wei, C.H. Hu, L. Rose, P. Karangwa, J. Yang, G.M. Deng, S.W. Liu, J. Gao, A. Viljoen, G.J. Yi, Fungal Genom. Biol. 3 (2013) 1—6.
[7] M. Dita, M. Barquero, D. Heck, E.S. Mizubuti, C.P. Staver, Front. Plant Sci. 9 (2018) 1—21.
[8] R.S. Goswami, H.C. Kistler, Mol. Plant Pathol. 5 (2004) 515—525.
[9] Z. Kang, I. Zingen-Sell, H. Buchenauer, Eur. J. Plant Pathol. 111 (2005) 19—28.
[10] A.R. Ola, D. Thomy, D. Lai, H. Brötz-Oesterhelt, P. Proksch, J. Nat. Prod. 76 (2013) 2094—2099.
[11] S. Liu, H. Dai, R.S. Orfali, W. Lin, Z. Liu, P. Proksch, J. Agric. Food Chem. 64 (2016) 3127—3132.
[12] W.-X. Wang, S. Kusari, S. Sezgin, M. Lamshöft, P. Kusari, O. Kayser, M. Spiteller, Appl. Microbiol. Biotechnol. 99 (2015) 7651—7662.
[13] J.C. Lee, E. Lobkovsky, N.B. Pliam, G. Strobel, J. Clardy, J. Org. Chem. 60 (1995) 7076—7077.
[14] J. Kornsakulkarn, K. Dolsophon, N. Boonyuen, T. Boonruangprapa, P. Rachtawee, S. Prabpai, P. Kongsaeree, Tetrahedron 67 (2011) 7540—7547.
[15] C. Yan, W. Liu, J. Li, Y. Deng, S. Chen, H. Liu, RSC Adv. 8 (2018) 14823—14828.
[16] J. Chen, X. Bai, Y. Hua, H. Zhang, H. Wang, Fitoterapia 134 (2019) 1—4.
[17] J. Gong, C. Chen, S. Mo, J. Liu, W. Wang, Y. Zang, H. Li, C. Chai, H. Zhu, Z. Hu,

J. Wang, Y. Zhang, Org. Biomol. Chem. 17 (2019) 5526–5532.
[18] Y. Shiono, M. Tsuchinari, K. Shimanuki, T. Miyajima, T. Murayama, T. Koseki, H. Laatsch, T. Funakoshi, K. Takanami, K. Suzuki, J. Antibiot. 60 (2007) 309–316.
[19] J.L. Sørensen, T.E. Sondergaard, L. Covarelli, P.R. Fuertes, F.T. Hansen, R.J.N. Frandsen, W. Saei, M.B. Lukassen, R. Wimmer, K.F. Nielsen, D.M. Gardiner, H. Giese, J. Nat. Prod. 77 (2014) 2619–2625.
[20] R.D. Wollenberg, T.E. Sondergaard, M.R. Nielsen, S. Knutsson, T.B. Pedersen, K.R. Westphal, R. Wimmer, D.M. Gardiner, J.L. Sørensen, Fungal Biol 123 (2019) 10–17.
[21] C.J. Thibodeaux, W. -c. Chang, H. -w. Liu, Chem. Rev. 112 (2012) 1681–1709.
[22] A. Andolfi, A. Boari, M. Evidente, A. Cimmino, M. Vurro, G. Ash, A. Evidente, J. Nat. Prod. 78 (2015) 623–629.
[23] N.P. Ariantari, G. Daletos, A. Mándi, T. Kurtán, W.E.G. Müller, W. Lin, E. Ancheeva, P. Proksch, RSC Adv. 9 (2019) 25119–25132.
[24] M. Solfrizzo, A. Visconti, M.E. Savard, B.A. Blackwell, P.E. Nelson, Mycopathologia 127 (1994) 95–101.
[25] J.M. Seco, E. Quinoá, R. Riguera, Chem. Rev. 104 (2004) 17–117.
[26] J. Lin, X. Chen, X. Cai, X. Yu, X. Liu, Y. Cao, Y. Che, J. Nat. Prod. 74 (2011) 1798–1804.
[27] J.G. Graham, H. Zhang, S.L. Pendland, B.D. Santarsiero, A.D. Mesecar, F. Cabieses, N.R. Farnsworth, J. Nat. Prod. 67 (2004) 225–227.
[28] A. Branco, A.C. Pinto, R. Braz-Filho, E.F. Silva, N.F. Grynberg, A. Echevarria, Rev. Bras. Farmacogn. 18 (2008) 703–708.
[29] W. Wätjen, A. Debbab, A. Hohlfeld, Y. Chovolou, A. Kampkötter, R.A. Edrada, R. Ebel, A. Hakiki, M. Mosaddak, F. Totzke, M.H.G. Kubbutat, P. Proksch, Mol. Nutr. Food Res. 53 (2009) 431–440.
[30] J. -p. Wang, A. Debbab, C.F.P. Hemphill, P.Z. Proksch, Naturforscher 68c (2013) 223–230.
[31] M. Moussa, W. Ebrahim, M. Bonus, H. Gohlke, A. Mándi, T. Kurtán, R. Hartmann, R. Kalscheuer, W. Lin, Z. Liu, P. Proksch, RSC Adv. 9 (2019) 1491–1500.
[32] E. Cho, M. Cai, H. Kwon, J. Jeon, M. Moon, M. Jun, Y.C. Lee, J.H. Yi, J.H. Ryu, D.H. Kim, Food Chem. Toxicol. 132 (2019) 1–7.
[33] P. Paudel, S.H. Seong, H.A. Jung, J.S. Choi, ACS Omega 4 (2019) 11621–11630.
[34] K. Suzuki, K. Nagao, Y. Monnai, A. Yagi, M. Uyeda, J. Antibiot. 51 (1998) 991–998.
[35] K. Suzuki, S. Yahara, Y. Kido, K. Nagao, Y. Hatano, M. Uyeda, J. Antibiot. 51 (1998) 999–1003.
[36] K. Suzuki, M. Yamaizumi, S. Tateishi, Y. Monnai, M. Uyeda, J. Antibiot. 52 (1999) 460–465.
[37] T. Sugawara, A. Tanaka, K. Tanaka, K. Nagai, K. Suzuki, T. Suzuki, J. Antibiot. 51 (1998) 435–438.
[38] L.W. MacIntyre, D.H. Marchbank, H. Correa, R.G. Kerr, J. Nat. Prod. 81 (2018) 2768–2772.
[39] J. Kjer, A. Debbab, A.H. Aly, P. Proksch, Nat. Protoc. 5 (2010) 479–490.
[40] T.R. Hoye, C.S. Jeffrey, F. Shao, Nat. Protoc. 2 (2007) 2451–2458.
[41] S. Vijayasarathy, P. Prasad, L.J. Fremlin, R. Ratnayake, A.A. Salim, Z. Khalil, R.J. Capon, J. Nat. Prod. 79 (2016) 421–427.
[42] M. Frank, F.C. Özkaya, W.E.G. Müller, A. Hamacher, M.U. Kassack, W. Lin, Z. Liu, P. Proksch, Mar. Drugs 17 (2019) 1–13.
[43] Apex2, Data Collection Program for the CCD Area-Detector System; SAINT, Data Reduction, Frame Integration Program for the CCD Area-Detector System, Bruker Analytical X-ray Systems, Madison, WI, USA, 1997–2012.
[44] G. Sheldrick, Program for Empirical Absorption Correction of Area Detector Data, University of Göttingen, Germany, 1996.
[45] G.M. Sheldrick, Acta Crystallogr. A 71 (2015) 3–8.
[46] G.M. Sheldrick, Acta Crystallogr. C 71 (2015) 3–8.
[47] H.D. Flack, G. Bernardinelli, Acta Crystallogr. A 55 (1999) 908–915.
[48] H.D. Flack, Acta Crystallogr. A 39 (1983) 876–881.
[49] R.W.W. Hooft, L.H. Straver, A.L. Spek, J. Appl. Crystallogr. 41 (2008) 96–103.
[50] K. Diamond Brandenburg, Crystal and Molecular Structure Visualization, 2009. Bonn, Germany, Version 3.2.
[51] A.L. Spek, Acta Crystallogr. D 65 (2009) 148–155.
[52] A.L. Spek, PLATON - A Multipurpose Crystallographic Tool, 2008. Utrecht, The Netherlands.
[53] L.J. Farrugia, Windows Implementation, Version 40608, University of Glasgow, Scotland, 2008.
[54] N.P. Ariantari, E. Ancheeva, M. Frank, F. Stuhldreier, D. Meier, Y. Gröner, I. Reimche, N. Teusch, S. Wesselborg, W.E.G. Müller, R. Kalscheuer, Z. Liu, P. Proksch, RSC Adv. 10 (2020) 7232–7240.
[55] CLSI, Methods for Dilution Antimicrobial Susceptibility Tests for Bacteria that Grow Aerobically, Approved Standard Ninth Ed. CLSI Document M07-A9, Clinical and Laboratory Standards Institute, Wayne, PA, 2012.
[56] N. Rehberg, E. Omeje, S.S. Ebada, L. van Geelen, Z. Liu, P. Sureechatchayan, M.U. Kassack, T.R. Ioerger, P. Proksch, R. Kalscheuer, Antimicrob. Agents Chemother. 63 (2019) e00136–19.